ACS central science

Research Article

Cite This: ACS Cent. Sci. 2018, 4, 1045−1055

Surveillance of Cancer Stem Cell Plasticity Using an Isoform-Selective Fluorescent Probe for Aldehyde Dehydrogenase 1A1

Chelsea Anorma,[†,▽] Jamila Hedhli,[‡,#,▽] Thomas E. Bearrood,[†,▽] Nicholas W. Pino,[†] Sarah H. Gardner,[§] Hiroshi Inaba,[†] Pamela Zhang,[†] Yanfen Li,[‡] Daven Feng,[†] Sara E. Dibrell,[†] Kristopher A. Kilian,[‡,∥] Lawrence W. Dobrucki,[‡,#] Timothy M. Fan,[⊥] and Jefferson Chan*[,†,§,#]

[†]Department of Chemistry and [§]Department of Biochemistry, University of Illinois at Urbana−Champaign, 600 S. Mathews Avenue, Urbana, Illinois 61801, United States

[‡]Department of Bioengineering, University of Illinois at Urbana−Champaign, 1304 W. Springfield Avenue, Urbana, Illinois 61801, United States

[∥]School of Materials Science and Engineering, School of Chemistry, University of New South Wales, Sydney, New South Wales 2052, Australia

[⊥]Department of Veterinary Clinical Medicine, University of Illinois at Urbana−Champaign, 2001 S Lincoln Avenue, Urbana, Illinois 61801, United States

[#]Beckman Institute for Advanced Science and Technology, University of Illinois at Urbana−Champaign, 405 N. Mathews Avenue, Urbana, Illinois 61801, United States

Supporting Information

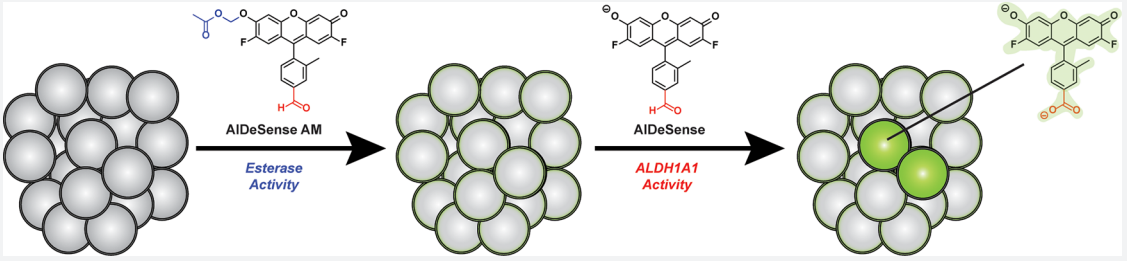

ABSTRACT: Cancer stem cells (CSCs) are progenitor cells that contribute to treatment-resistant phenotypes during relapse. CSCs exist in specific tissue microenvironments that cell cultures and more complex models cannot mimic. Therefore, the development of new approaches that can detect CSCs and report on specific properties (e.g., stem cell plasticity) in their native environment have profound implications for studying CSC biology. Herein, we present AlDeSense, a turn-on fluorescent probe for aldehyde dehydrogenase 1A1 (ALDH1A1) and Ctrl-AlDeSense, a matching nonresponsive reagent. Although ALDH1A1 contributes to the detoxification of reactive aldehydes, it is also associated with stemness and is highly elevated in CSCs. AlDeSense exhibits a 20-fold fluorescent enhancement when treated with ALDH1A1. Moreover, we established that AlDeSense is selective against a panel of common ALDH isoforms and exhibits exquisite chemostability against a collection of biologically relevant species. Through the application of surface marker antibody staining, tumorsphere assays, and assessment of tumorigenicity, we demonstrate that cells exhibiting high AlDeSense signal intensity have properties of CSCs. Using these probes in tandem, we have identified CSCs at the cellular level via flow cytometry and confocal imaging, as well as monitored their states in animal models.

INTRODUCTION

Cancer stem cells (CSCs) were first discovered in human acute myelogenous leukemia[1] and have since been identified in breast cancer, glioblastoma, multiple myeloma, gastric cancer, pancreatic cancer, and colon cancer, among others.[2] CSCs have an increased capacity to activate antiapoptotic and pro-survival pathways, as well as to overexpress ATP-binding cassette transporters which act as potent efflux pumps to extrude small molecules (e.g., chemotherapeutics) from the cancer cells.[3,4] As such, conventional chemotherapeutics can inadvertently lead to an enrichment of CSCs by killing non-CSCs, which in turn contributes to the emergence of highly aggressive and treatment-resistant phenotypes during relapse.[5] Unfortunately, the behavior of CSCs, especially in an in vivo context, is insufficiently understood despite the availability of cell cultures and three-dimensional (3D) models. A major drawback of these systems is that they cannot mimic the complex microenvironment where CSCs are thought to reside. Moreover, CSCs are rare and represent only a small fraction of

Received: May 16, 2018
Published: July 25, 2018

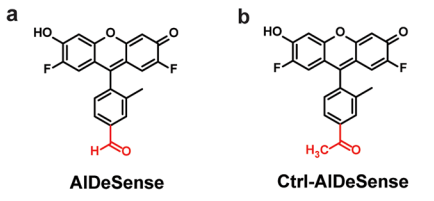

c

Compound	λ_{abs} (nm)	λ_{em} (nm)	ε ($M^{-1}cm^{-1}$)	Φ_F	pKa	Log $D_{7.4}$	Turn-on (fold)
AlDeSense	496	516	6.1×10^4	0.041	4.81	0.88	20.0
Ctrl-AlDeSense	496	518	6.8×10^4	0.039	4.47	0.87	0

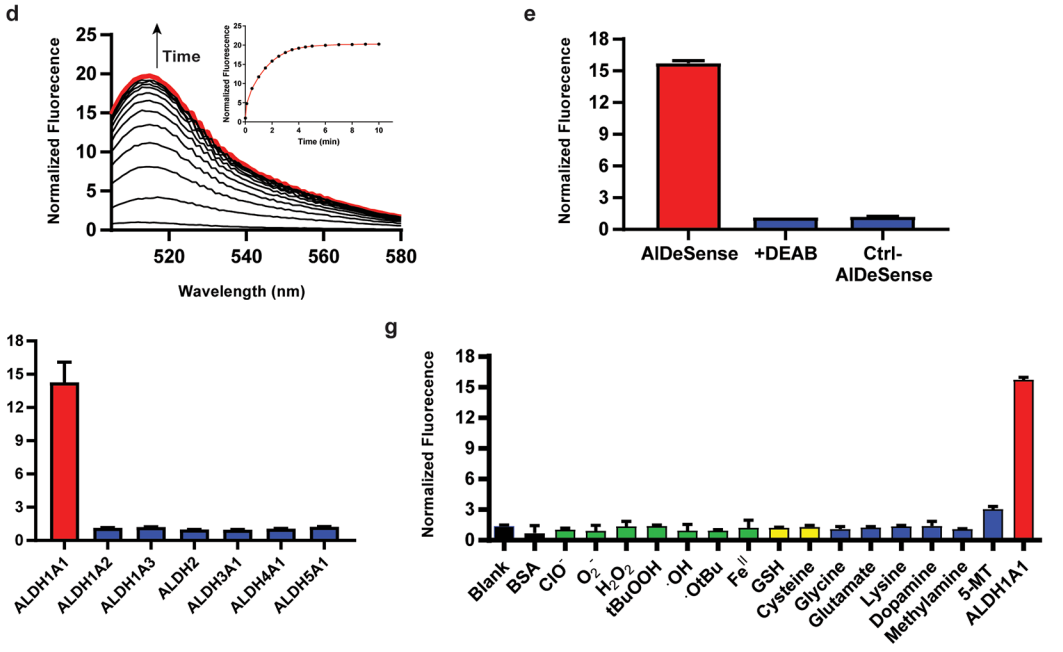

Figure 1. Chemical structures of (a) AlDeSense and (b) Ctrl-AlDeSense. (c) Comparison of photophysical and chemical properties of AlDeSense and Ctrl-AlDeSense. (d) Fluorescence spectra of AlDeSense upon incubation with recombinant ALDH1A1 at room temperature. Inset shows fluorescence increase over time under the same conditions. (e) Comparison of fluorescence signal from ALDH1A1 reacting with the following: AlDeSense, AlDeSense with additional inhibition with DEAB (100 nM), and Ctrl-AlDeSense. (f) Normalized fluorescence turn-on of AlDeSense after incubation with 20 units of each ALDH isoform for 30 min at room temperature. Units are defined as 1 μmol of substrate turned over/μmol enzyme/min. (g) Response of AlDeSense to various reactive oxygen species, biological thiols, and amines at concentrations of 100 μM (GSH was tested at 1 mM). For all assays, AlDeSense was used at 1 μM final concentration.

cells within a tumor. CSCs also exist in a dynamic equilibrium between undifferentiated and differentiated states,[6] which is modulated by specific properties of the tumor microenvironment (e.g., hypoxia), as well as interactions with a network of cells, signaling molecules, and the extracellular matrix.[7−9] Thus, methods that can be employed to not only detect CSCs but also to report on specific in vivo properties such as stem cell plasticity are highly desirable. One approach to image CSCs is to target CSC surface biomarkers with a reporter (e.g., optical dye) conjugated to an antibody.[10] However, this can lead to off-target binding[11] and uneven or incomplete staining because antibody−dye conjugates cannot readily permeate into tumor regions distal from blood vasculature.[12,13] Alternatively, genetically engineered CSCs expressing fluorescent proteins (e.g., GFP) or luciferase bioluminescent constructs can facilitate lineage tracing experiments.[14−16] Major limitations are that it can only be used to visualize CSCs that have been previously isolated, transfected, and reintroduced into an animal model, but not all cell types are amenable to genetic manipulation.

In contrast, aldehyde dehydrogenases (ALDHs), in particular, the 1A1 isoform, is believed to be a reliable marker of CSCs across many cancer types, including prostate, lung, breast, esophageal, and ovarian cancers.[17−22] In these instances, ALDH1A1 is associated with treatment resistance and poor clinical outcome. In addition to ALDH1A1, there are 18 other ALDH isoforms in humans, many of which display promiscuous and overlapping substrate scopes with ALDH1A1 when catalyzing the oxidation of endogenous and xenobiotic aldehydes to the corresponding carboxylic acid products.[23,24] Although challenging, the development of a selective activity-based fluorescent probe for ALDH1A1 would enable detection of CSCs, as well as concurrently report on their degree of stemness. In this regard, there is a gradient of ALDH1A1 activity ranging from high in CSCs to low in differentiated cancer cells (infra vide). Several probes have been developed for ALDH, including BODIPY-aminoacetaldehyde (BAAA).[25−27] However, these examples suffer from major drawbacks. Because BAAA is equally fluorescent compared to its turned-over carboxylate product, CSCs are identified based on their ability to retain the BAAA product relative to the unactivated probe using efflux pump inhibitors. Additionally, an ALDH inhibitor (i.e., *N*,*N*-diethylaminobenzaldehyde (DEAB)) must also be used in tandem to distinguish between signal from ALDH activity and nonspecific accumulation in cells.[28,29] While these are useful tools for isolating CSCs from solid tumors and cell cultures, introduction of efflux pump and ALDH inhibitors to live animals will have unintended consequences. More importantly, BAAA exhibits cross-reactivity with several ALDH isoforms rendering the

DOI: 10.1021/acscentsci.8b00313
ACS Cent. Sci. 2018, 4, 1045−1055

interpretation of experimental results challenging.[18,30,31] Herein, we describe the development of a highly selective, activity-based fluorescent probe to target elevated ALDH1A1 in CSCs. Through the application of established protocols that include identifying CSC surface markers, cultivation of tumorspheres, and assessment of tumorigenicity, we provide evidence that the brightest AlDeSense cells possess CSC properties. Finally, we employ our probe to monitor CSC plasticity in a tumor model using live mice.

RESULTS

Design and Synthesis of AlDeSense. Our ALDH1A1 probe, AlDeSense, is based on the photostable Pennsylvania Green dye platform and is equipped with a pendant benzaldehyde moiety (Figure 1a).[32] Electron deficient aryl groups such as benzaldehyde can attenuate fluorescence via the donor-photoinduced electron transfer (d-PeT) quenching mechanism.[33,34] This provides the desired signal enhancement upon conversion to the unquenched carboxylic acid by ALDH1A1. We rationally selected the Pennsylvania Green scaffold because at physiological pH it is negatively charged (apparent pK_a = 4.81). The negative charge on the dye is expected to negate the need for efflux pump inhibitors because the turned-over product will be dianionic and less able to cross the cell membrane.[35] The low pK_a serves a second purpose since it can presumably form an ionic interaction with His-293 located at the entrance of the active site (Figure S1).[36] This imparts selectivity against isoforms such as ALDH1A3 where the corresponding His residue is not present.[37−39] As predicted by the literature, the benzaldehyde moiety will also augment isoform selectivity, since benzaldehydes are better substrates for ALDH1A1 than many of the other ALDH isoforms.[40] Despite the fact that AlDeSense is weakly fluorescent until activated, nonspecific staining can still contribute to misidentification of non-CSC populations. To account for this and circumvent the need for ALDH inhibitors, we developed Ctrl-AlDeSense, a nonresponsive matching control reagent (Figure 1b). Although Ctrl-AlDeSense is structurally similar to AlDeSense and displays nearly identical physical properties, replacing the benzaldehyde moiety with an acetophenone group renders it unreactive to ALDH1A1 (Figure 1c, Figures S2 and S3).

The synthesis of AlDeSense involved DIBAL reduction of methyl 4-bromo-3-methylbenzoate **1** to afford the corresponding benzyl alcohol , which was protected with *tert*-butyldimethylsilyl chloride to give **2** in 93% yield over two steps. Lithium halogen exchange enabled coupling to MEM-protected difluoroxanthone **3** giving the Pennsylvania Green intermediate **4** in 48% yield after acid mediated global deprotection. IBX oxidation of the benzyl alcohol then afforded AlDeSense in 79% yield. Preparation of AlDeSense AM, a cell permeable derivative, could be achieved via alkylation of AlDeSense with bromomethyl acetate in 60% yield (Scheme 1). Once internalized, intracellular esterases can hydrolyze the AM group to afford the parent AlDeSense reagent. The synthesis of Ctrl-AlDeSense involved similar chemistry, and the details can be found in the Supporting Information. Of note, both AlDeSense and AlDeSense AM will herein be referred to as AlDeSense for simplicity. AM protected versions were utilized for all cellular and animal studies.

In Vitro Characterization. With AlDeSense in hand, we first evaluated its response to purified ALDH1A1. Prior to activation, AlDeSense was weakly fluorescent (Φ_F = 0.04);

Scheme 1. Synthesis of AlDeSense and AlDeSense AM

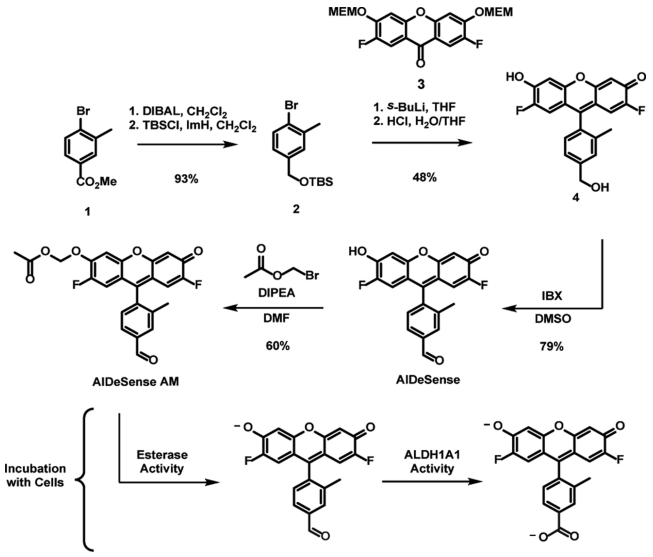

however, addition of ALDH1A1 resulted in a robust ∼20-fold fluorescent enhancement (Figure 1d). Inhibition of ALDH1A1 with DEAB completely abolished the turn-on response, and the resulting fluorescent signal was comparable to that of Ctrl-AlDeSense (Figures 1e and S4). Next, we screened for potential cross-reactivity against a panel of the most common ALDH isoforms and found that only ALDH1A1 led to probe activation (Figures 1f and S5). To ensure that AlDeSense is only activated by ALDH1A1 when in cells, we assessed potential off-target responses against various biologically relevant analytes. Although aldehyde groups are prone to oxidation, we did not observe any oxidized fluorescent products when screened against a panel of reactive oxygen species (Figure 1g). Similarly, when AlDeSense was incubated with various thiols and amines, we did not detect formation of fluorescent hemithioacetal[41,42] and Schiff base[43] products, respectively (Figure 1g). We also established that AlDeSense, its turned-over product, and the control reagent are nontoxic using standard cell viability assays (Figure S6). Moreover, LC-MS shows that AM deprotection, as well as ALDH1A1-catalyzed oxidation occurs upon cell uptake (Figure S7). Together, these key experiments indicate that AlDeSense is suitable for detecting ALDH1A1 activity in living systems.

Detection of ALDH1A1 Activity in K562 Cells. To investigate the ALDH1A1 sensing capabilities of AlDeSense in cell culture, we utilized the K562 human chronic myeloid leukemia cell line, which is known to exhibit high overall ALDH activity.[44] We hypothesized that AlDeSense can be used to stratify these cells based on ALDH1A1 activity and that the brightest cells would exhibit CSC markers. First, using flow cytometry analysis, we found that K562 cells stained with AlDeSense are significantly brighter compared to those treated with either AlDeSense with an inhibitor or Ctrl-AlDeSense (Figures 2a−c and S8). We also identified a population of AlDeSense positive cells that exhibits the CD34+/CD38- profile characteristic of leukemic stem cells. The relative proportion of these cells increased when K562 cells were cultured under an environment low in oxygen (Figure S9). Exposure to hypoxia is a common condition to enrich for CSCs.[45,46] We also assessed the utility of AlDeSense for confocal fluorescence imaging, which in contrast to flow

DOI: 10.1021/acscentsci.8b00313
ACS Cent. Sci. 2018, 4, 1045−1055

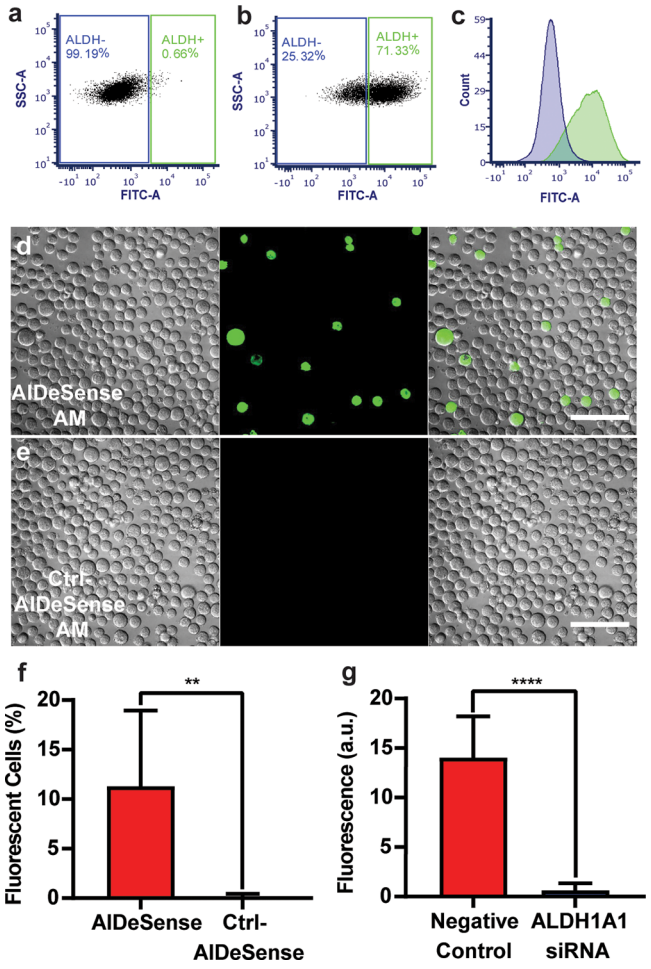

Figure 2. Application of AlDeSense and Ctrl-AlDeSense in live K562 cells. Flow cytometry analysis of K562 cells stained with (a) Ctrl-AlDeSense (1.5 μM) or (b) AlDeSense (1.5 μM). (c) Histographic profiles of (a) and (b) shown in blue and green, respectively. Confocal images of K562 cells stained with (d) AlDeSense or (e) Ctrl-AlDeSense both at 2 μM. Scale bars are 100 μm. (f) Percentage of total cells showing fluorescence using each of these stains. (Error bars are ± SD, n = 9, unpaired t test with Welch's correction.) (g) Knockdown of ALDH1A1 using siRNA showed an ablation of signal compared to cells treated with a scrambled siRNA as a negative control. (Error bars are SD, n = 15, unpaired t test with Welch's correction.)

cytometry, requires less sample and allows for visual assessment of cell morphology (Figure 2d). First, we determined the subcellular staining pattern of AlDeSense. ALDH1A1 is a cytoplasmic enzyme, and therefore, AlDeSense should not be localized to organelles such as the mitochondria where other ALDH isoforms (e.g., ALDH2) are present at high abundance. Co-staining with organelle-specific trackers revealed that AlDeSense did in fact stain the cytoplasm and was not extensively localized to various organelles (Figures S10 and S11). After several minutes, a small population of highly fluorescent cells began to emerge owing to ALDH1A1-mediated activation of our probe. Treatment with an ALDH inhibitor as well as ALDH1A1-specific siRNA knockdown confirmed that ALDH1A1 is responsible for the fluorescence enhancement (Figures 2g, S12, S13). Further confirmation of in cellulo selectivity was obtained by comparing K562 cells with HEK293T cells, an ALDH1A1 negative cell line (Figure S14).[47] Cells treated with Ctrl-AlDeSense allowed us to establish baseline microscope settings which account for fluorescence due to accumulation of dye (Figure S15). Applying these settings to the AlDeSense-stained population, any cell which shows fluorescence above baseline can only be due to the ALDH1A1-catalyzed turnover of AlDeSense (Figure 2d–f). Of note, the brightest cells also displayed the CD34+/CD38-/CD133+ leukemic stem cell profile (Figure S16), suggesting that AlDeSense was being activated to the greatest extent in putative CSCs.

Identification of CSCs in Cell Culture Using AlDeSense. Next, we sought to determine whether our probe would yield greater fluorescence in CSCs obtained using two different enrichment strategies. First, we used the well-established mammosphere assay to cultivate MDA-MB-231 CSCs by growing cells in low serum conditions on non-adherent plates.[48] Under these conditions, non-CSCs die off, leaving individual CSCs to proliferate into spherical structures. Mammospheres as well as tumorspheres derived from other cancer types have been shown to generate cells with nearly all known CSC characteristics—such as increased in vivo tumorigenicity, invasiveness, metastasis rates, EMT transition, and resistance to chemotherapeutics. Thus, they are widely used to study CSCs and develop CSC-specific therapeutics.[49] Mammospheres stained with AlDeSense were 3-fold brighter than those stained with Ctrl-AlDeSense, showing increased levels of ALDH1A1 activity in the mammospheres. In addition, transferring the mammospheres to normal cell culture media and allowing them to differentiate led to a gradual decrease of AlDeSense signal over 36 h, demonstrating that AlDeSense can be used to monitor CSC differentiation (Figure 3a–e).

For the second model in our study, we chose to enrich CSCs using a protocol recently published by Kilian and co-workers,[50] where they reported that B16F0 melanoma cells cultured on a spiral-patterned hydrogel platform to mimic mechanical properties of the tumor microenvironment gave rise to cells that displayed increased CSC marker expression (e.g., CD271), as well as metastatic potency and tumorigenicity. Only a small fraction of the B16F0 cells cultured under standard conditions were identified to exhibit elevated ALDH1A1 activity via flow cytometry and confocal imaging using AlDeSense. However, when the cells enriched in CSCs via the patterned platform (herein referred as e-CSCs) were treated with AlDeSense, they were 11.3-fold brighter than those grown under standard conditions (referred herein as non-CSCs). e-CSCs treated with AlDeSense were also 9.0-fold brighter than e-CSCs treated with Ctrl-AlDeSense, demonstrating that the signal was due to ALDH1A1 (Figure 3f–j). Flow cytometry analysis revealed that e-CSCs displayed colocalization of AlDeSense with CD271, a commonly used melanoma stem cell marker, when compared to non-CSCs (Figure S17).[51,52]

Ex Vivo Imaging of ALDH1A1 Activity in e-CSCs. We subsequently sought to visualize ALDH1A1 activity in e-CSCs introduced into whole animal models. First, we intravenously injected either e-CSCs or non-CSCs into mice via the tail vein to generate metastatic lesions in the lung. Immunocompetent mice were used with this syngeneic cell line because the immune system is known to influence the tumor microenvironment and hence properties of CSCs in vivo.[11] Since e-CSCs lost many of the stem cell-related properties within 5 days after they were replated on glass slides,[50] it was essential to determine whether ALDH1A1 activity was maintained after

DOI: 10.1021/acscentsci.8b00313
ACS Cent. Sci. 2018, 4, 1045–1055

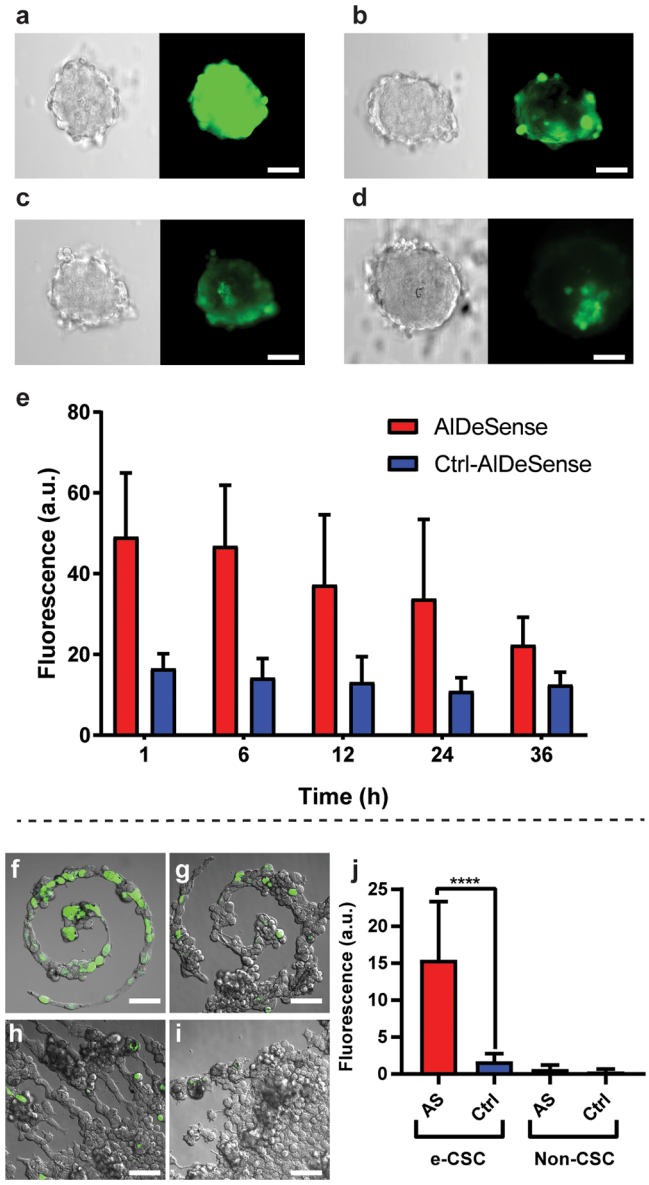

Figure 3. Imaging of enriched-CSC cell cultures. Representative brightfield and fluorescence images of mammospheres stained with (a) AlDeSense and (b) Ctrl-AlDeSense. Representative brightfield and fluorescence images of mammospheres after 36 h in normal cell culture media, stained with (c) AlDeSense and (d) Ctrl-AlDeSense. (e) Mean fluorescence signals from mammospheres for both dyes at several time points throughout differentiation. Error bars are ± SD, $n \geq 7$. Confocal imaging of patterned (e-CSC) B16F0 melanoma versus nonpatterned (non-CSC) melanoma using AlDeSense (AS) and Ctrl-AlDeSense (Ctrl). Representative composite brightfield and fluorescence images of (f) e-CSCs stained with AlDeSense, (g) e-CSCs stained with Ctrl-AlDeSense, (h) non-CSCs stained with AlDeSense, and (i) non-CSCs stained with Ctrl-AlDeSense. Quantification of the fluorescence intensity (j). For each condition, $n \geq 21$ images were taken across three different sample preparations. Error bars are ± SD. Scale bars are 50 μm.

CSCs were introduced into a living system. Specifically, can metastatic niches be established within this time frame before differentiation takes place? We hypothesized that if e-CSCs retained their stemness, the AlDeSense signal would be higher for e-CSC lungs compared to non-CSC lungs. At various time points during tumor progression (day 7 and 11) mice were sacrificed, their lungs were removed and perfused with solutions of either AlDeSense or Ctrl-AlDeSense (Figure 4a–d). When stained with AlDeSense, the fluorescence of the

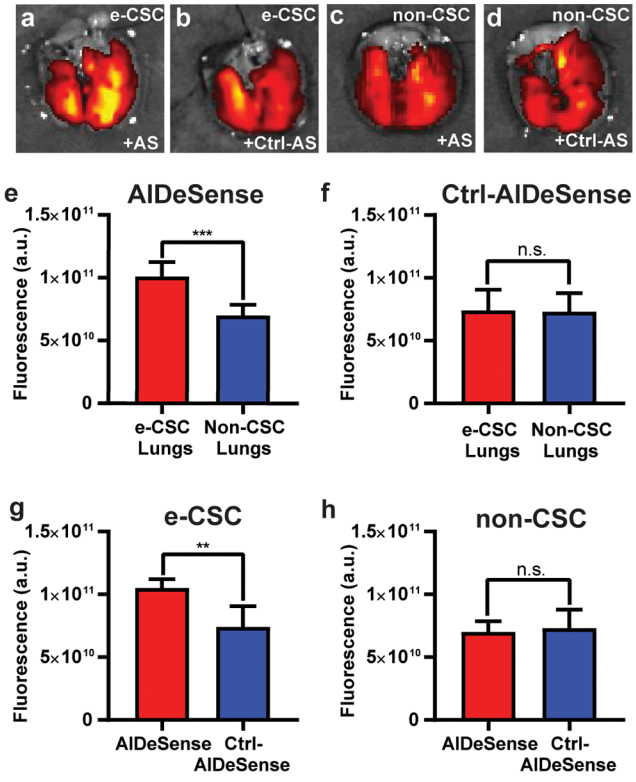

Figure 4. Assessment of AlDeSense in murine melanoma models. Representative images of lungs collected at day 11 with (a) e-CSC metastases stained with AlDeSense (AS), (b) e-CSC metastases stained with Ctrl-AlDeSense (Ctrl-AS), (c) non-CSC metastases stained with AlDeSense, and (d) non-CSC metastases stained with Ctrl-AlDeSense, all displayed as bright field images overlaid with fluorescence signal. Staining with AlDeSense (e) led to a significant difference in signal between e-CSC metastases and non-CSC metastases, but staining with Ctrl-AlDeSense (f) did not show a difference between e-CSC and non-CSC. When analyzing the e-CSC samples, AlDeSense showed a significant increase in signal in comparison to Ctrl-AlDeSense (g). This difference was not observed when analyzing non-CSC samples (h). For panels (e–h) error bars are ± SD, $n \geq 4$ for each condition.

e-CSC-treated lungs was indeed higher than the signal from non-CSC-treated lungs (Figure 4e). However, it is possible that e-CSCs simply gave rise to larger metastatic lesions which could uptake more dye, leading to increased fluorescence intensity. To resolve this, we compared the signal of e-CSC and non-CSC lungs stained with Ctrl-AlDeSense and found that they were not statistically different, allowing us to confidently rule out this as a possibility (Figure 4f). Moreover, e-CSC lungs also had a higher signal from AlDeSense versus Ctrl-AlDeSense (Figure 4g). On the other hand, differences in intensity were not observed between AlDeSense and Ctrl-AlDeSense in lungs with non-CSC metastases (Figure 4h). Results from days 7 and 11 showed consistent patterns (Figure S18). Taken together, these results demonstrate that the e-CSCs continue to have higher ALDH1A1 activity levels after introduction into a living system, and that AlDeSense in conjunction with Ctrl-AlDeSense can be used to identify e-CSCs exhibiting this activity.

DOI: 10.1021/acscentsci.8b00313
ACS Cent. Sci. 2018, 4, 1045–1055

In Vivo Imaging of ALDH1A1 Activity in e-CSCs Implanted into Live Animals. With this information in hand, we then evaluated the tumorigenicity of e-CSCs and the corresponding performance of AlDeSense in a live animal model. Allografts in BALB/c mice were generated via the subcutaneous injection of e-CSCs and non-CSCs into the right and left flanks, respectively. Tumors were monitored and imaged up to 2 weeks using a whole-body fluorescence imager following an intratumoral injection of AlDeSense or Ctrl-AlDeSense. Results revealed a consistently higher signal from AlDeSense in the e-CSCs versus non-CSCs tumors (Figure 5a–c) at both 1 and 2 weeks. Ctrl-AlDeSense, on the other hand, did not show increased signal from the e-CSC tumor and had much lower signal over all. This demonstrates that AlDeSense can be used to image ALDH1A1 activity in vivo, and more importantly that e-CSCs retained high ALDH1A1 activity after implantation and induction of tumorigenesis. Moreover, consistent with higher tumorgenicity, implantation of e-CSCs into mice yielded larger, more aggressive tumors compared to non-CSCs (Figure 5d).

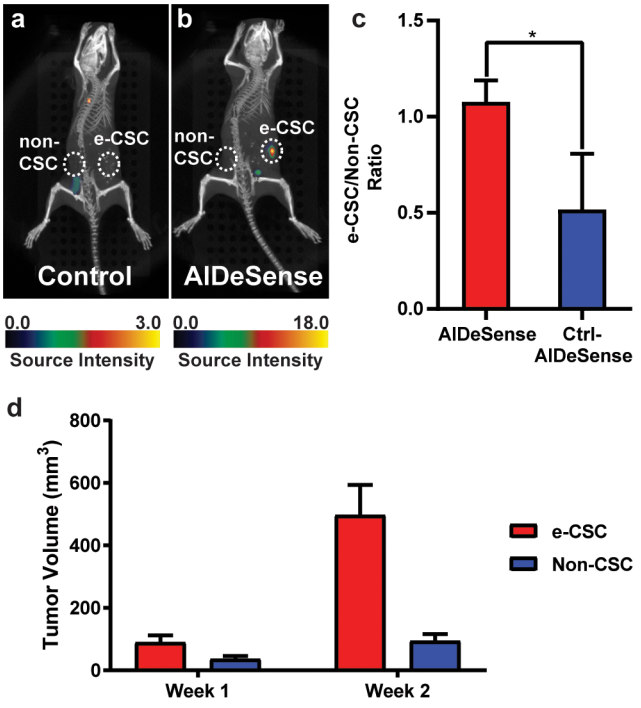

Figure 5. Representative images of mice implanted with both non-CSC and e-CSC tumors on either flank and injected with (a) Ctrl-AlDeSense or (b) AlDeSense intratumorally. Tumor regions are highlighted with white circles and fluorescence signal was overlaid over CT images to show placement of signal. (c) Ratio of signal from e-CSC/non-CSC tumors is shown for both Ctrl-AlDeSense and AlDeSense injections. Error bars are ± SD, n = 3 for each dye. (d) Mean volumes of both e-CSC and non-CSC tumors throughout the time course of the experiment. Error bars are ± SD, n = 5 for each tumor type.

DISCUSSION

In conclusion, we have developed AlDeSense, a powerful new turn-on fluorescent reagent optimized for the detection of CSCs and monitoring of stem cell plasticity via ALDH1A1 activity. Unactivated AlDeSense is weakly fluorescent owing to d-PeT quenching from the pendant benzaldehyde moiety; however, the fluorescence signal is enhanced by nearly 20-fold upon oxidation to the corresponding benzoic acid product by ALDH1A1. Importantly, we did not observe cross-reactivity with any of the other ALDH isoforms tested. This selectivity can be attributed to benzaldehyde being a better substrate for ALDH1A1 and a crucial ionic interaction that we postulate to be forming between the negatively charged dye scaffold and a positively charged His residue at the entrance of the ALDH1A1 active site. Attempts to elucidate the exact nature of this selectivity by cocrystallizing AlDeSense and ALDH1A1 were unsuccessful. The interaction between the active site cysteine residue (Cys-302) and AlDeSense results in a dynamic equilibrium between the aldehyde and hemithioacetal forms which creates too much disorder for crystallographic visualization of the complex. Nevertheless, the exquisite selectivity of AlDeSense for ALDH1A1 over other isoforms, as well as its excellent chemoselectivity against a panel of biologically relevant analytes ensures that any signal above the background established using Ctrl-AlDeSense is due to ALDH1A1 activity.

This property offers unique advantages over existing approaches such as those that involve antibody-dye conjugates for CSC imaging. Dyes that are appended to antibodies targeting CSCs are always in a fluorescent "on" state, meaning background signal will be high. In contrast, AlDeSense is weakly fluorescent until it is activated by ALDH1A1, and any nonspecific staining can be readily accounted for by employing the matching control reagent (Ctrl-AlDeSense). Another advantage is that our probe is compatible with many cancer cell types because elevated ALDH1A1 activity is a general property of CSCs. In contrast, CSC surface biomarkers are unique to specific cancers but are often ill-defined and heterogeneously displayed. Because AlDeSense is cell-permeable and acts intracellularly, it does not directly interfere with native cell-surface processes through formation of tight-binding antibody–antigen interactions, offering yet another advantage. Finally, AlDeSense will only activate if CSCs are viable because ALDH1A1 depends on availability of NADH. In contrast, CSCs that are no longer living can still display surface biomarkers. In comparison to BAAA, a nonselective commercial reagent designed to also target ALDH activity, AlDeSense is selective for only the ALDH1A1 isoform. BAAA on the other hand has been shown to react with a variety of isoforms, including ALDH1A2, ALDH1A3, ALDH2, and ALDH4A1, both in previous reports[18,30,31] and under our own examination (Figure S19). Furthermore, AlDeSense is a turn-on probe that localizes in the cytosol, while BAAA is accumulation-based and localizes to the ER and mitochondria (Figure S20). This means that unlike BAAA, AlDeSense does not require either ALDH or efflux pump inhibitors to selectively label CSCs and will not show false positives from mitochondrially-located ALDH isoforms, such as ALDH2.

Owing to the unique imaging capabilities of AlDeSense, CSCs enriched using various approaches can be imaged via confocal microscopy to approximate the degree of stemness versus the extent of differentiation. Indeed, we have demonstrated in this study through the application of surface marker antibody staining, tumorsphere assays, and assessment of tumorigenicity, that cells exhibiting high AlDeSense signal intensity have properties of CSCs. For both chronic myelogenous leukemia and melanoma, cells exhibiting the CSC markers CD34+/CD38-/CD133+ and CD271, respectively, were among the brightest cells when stained with AlDeSense. In addition to costaining with antibodies, we also

DOI: 10.1021/acscentsci.8b00313
ACS Cent. Sci. 2018, 4, 1045–1055

generated CSC-enriched mammospheres and showed that they displayed elevated ALDH1A1 activity. We also observed a decrease in ALDH1A1 activity by allowing the mammospheres to differentiate over time, demonstrating that AlDeSense could be used as a tool to monitor CSC plasticity. Lastly, we used AlDeSense to assess CSC plasticity after introduction into living systems.

Prior to this study, it was unknown whether e-CSCs would retain properties of stemness such as high ALDH1A1 activity after introduction into a living system. Our imaging experiments demonstrate that ALDH1A1 activity persists up to several weeks in e-CSCs after they are introduced into a living animal, implicating that a niche must be established that supports this population of cells. Current efforts will focus on employing AlDeSense to determine parameters of the tumor microenvironment that govern the transition from a differentiated to CSC state and vice versa. Future work will be focused on two fronts. First, we will develop red-shifted congeners to enable higher resolution imaging of CSCs in deeper tissues. Second, we will generate selective probes for other ALDH isoforms such as ALDH1A3 that are also believed to be linked to stemness. Beyond leading to a greater understanding of fundamental CSC biology, we envision that AlDeSense and other ALDH activity-based probes can be utilized as powerful prognostic indicators and assist in the development of CSC-specific chemotherapeutics.

EXPERIMENTAL DETAILS

((4-Bromo-3-methylbenzyl)oxy)(*tert*-butyl)-dimethylsilane (2). A flame-dried round-bottom flask was charged with methyl 4-bromo-3-methylbenzoate (11.5 g, 50.0 mmol, 1.00 equiv) and anhydrous CH_2Cl_2 (100 mL). A flame-dried addition funnel was attached to the flask and the system was flushed with nitrogen. The reaction was cooled to 0 °C and treated with 1.0 M DIBAL-H in CH_2Cl_2 (110 mL, 110 mmol, 2.2 equiv) via funnel addition over 23 min. The reaction was allowed to warm to room temperature. After stirring at room temperature for 4 h, the reaction was cooled to 0 °C and quenched via the slow addition of H_2O (5 mL), 1 M NaOH (5 mL), and additional H_2O (30 mL). The resulting emulsion was poured over filter paper and washed with CH_2Cl_2. The organics were combined, dried over Na_2SO_4, and concentrated under reduced pressure. The crude residue was eluted through a silica plug and concentrated to afford a light-yellow oil which was used without further purification. A solution of this intermediate in anhydrous CH_2Cl_2 (50 mL) was treated with imidazole (6.8 g, 100 mmol, 2.0 equiv) and *tert*-butyldimethylsilyl chloride (8.2 g, 55 mmol, 1.1 equiv). After overnight stirring, the reaction was filtered and washed with CH_2Cl_2. The filtrate was collected, washed with aqueous NH_4Cl, and concentrated under reduced pressure. The crude material was purified via flash chromatography on a silica column (2:98 v/v EtOAc/hexanes) to afford the title compound (14.6 g, 46.3 mmol, 92.6% yield over two-steps beginning from methyl 4-bromo-3-methylbenzoate). ^{1}H NMR (500 MHz, $CDCl_3$) δ 7.47 (d, J = 8.1 Hz, 1H), 7.18 (d, J = 1.6 Hz, 1H), 7.01 (dd, J = 8.2, 1.5 Hz, 1H), 4.66 (s, 2H), 2.39 (s, 3H), 0.94 (s, 9H), 0.10 (s, 6H). ^{13}C NMR (125 MHz, $CDCl_3$) δ 140.82, 137.67, 132.22, 128.63, 125.20, 123.15, 64.48, 26.09, 23.09, 18.57, −5.10.

2,7-Difluoro-3,6-bis((2-methoxyethoxy)methoxy)-9*H*-xanthen-9-one (3). The titled compound was prepared according the procedure published by Peterson and co-workers.[53]

2,7-Difluoro-6-hydroxy-9-(4-(hydroxymethyl)-2-methylphenyl)-3*H*-xanthen-3-one (4). A flame-dried round-bottom flask was charged with **2** (0.348 g, 1.1 mmol, 1.1 equiv) and anhydrous THF (5 mL). The reaction was cooled to −78 °C and treated with 1.4 M *sec*-butyllithium in cyclohexane (0.9 mL, 1.1 mmol, 1.1 equiv). The reaction was stirred at the same temperature for 30 min and then treated with a solution of **3** (0.440 g, 1.0 mmol, 1.0 equiv) in anhydrous THF (5 mL). The reaction was stirred at the same temperature for 2 h. The reaction was warmed to room temperature and treated with 1.0 M aq. HCl (6.0 mL, 6.0 mmol, 6.0 equiv). The reaction was warmed to 50 °C and stirred for 4 h. The reaction was concentrated under a vacuum to remove the THF and cyclohexane. The remaining mixture was poured over filter paper, washed with H_2O (100 mL) and CH_2Cl_2 (100 mL), and vacuum-dried to yield the title compound as a red-orange solid (0.176 g, 0.483 mmol, 48.3% yield). ^{1}H NMR (500 MHz, DMSO-d_6) δ 7.44 (s, 1H), 7.39 (d, J = 7.7 Hz, 1H), 7.23 (d, J = 7.7 Hz, 1H), 6.82 (d, J = 6.0 Hz, 2H), 6.59 (d, J = 11.3 Hz, 2H), 5.33 (s, 0H), 4.62 (s, 2H), 2.02 (s, 3H). ^{13}C NMR (125 MHz, DMSO-d_6) δ 150.29 (t, J = 6.1 Hz), 144.31, 135.32, 129.86, 128.71, 128.50, 124.21, 114.00, 111.28 (d, J = 21.9 Hz), 105.06 (d, J = 4.3 Hz), 62.52, 19.11. HRMS-ESI (m/z): $[M + H]^+$ Calc. mass for $C_{21}H_{15}O_4F_2$ = 369.0938; Found mass = 369.0930.

AlDeSense. A round-bottom flask was charged with **4** (0.368 g, 1.0 mmol, 1.0 equiv), IBX (0.336 g, 1.2 mmol, 1.2 equiv), and DMSO (10 mL). After being stirred for 3 h at room temperature, the reaction was quenched via the addition of brine (100 mL). The resulting mixture was poured over filter paper and vacuum-dried. The red solid was suspended in H_2O (200 mL) and heated to 80 °C. After stirring for 2 h, the reaction was cooled to room temperature and poured over filter paper and vacuum-dried to yield the title compound as a rust-orange solid (0.290 g, 0.79.2 mmol, 79.2% yield). AlDeSense used in biological assays was further purified via chromatography on a silica column (10:90 v/v MeOH:CH_2Cl_2). ^{1}H NMR (500 MHz, DMSO-d_6) δ 10.12 (s, 1H), 8.02 (s, 1H), 7.95 (d, J = 7.8 Hz, 1H), 7.52 (d, J = 7.6 Hz, 1H), 6.80 (d, J = 6.8 Hz, 1H), 6.60 (d, J = 11.4 Hz, 2H), 2.12 (s, 3H). ^{13}C NMR (125 MHz, DMSO-d_6) δ 193.01, 154.48, 154.28, 152.48, 148.77 (t, J = 5.7 Hz), 138.57, 136.95, 136.83, 131.32, 129.88, 127.32, 110.11 (d, J = 21.7 Hz), 109.50 (d, J = 8.2 Hz), 104.93 (d, J = 5.4 Hz), 18.90. $[M + H]^+$ Calc. mass for $C_{21}H_{13}O_4F_2$ = 367.0782; Found mass = 367.0784.

AlDeSense AM. A flame-dried round-bottom flask was charged with AlDeSense (0.037 g, 0.10 mmol, 1.0 equiv), anhydrous DMF (2.0 mL), bromomethyl acetate (0.020 mL, 0.20 mmol, 2.0 equiv), and Hünig's base (0.035 mL, 0.20 mmol, 2.0 equiv). After being stirred for 12 h at room temperature, all volatiles were removed under a vacuum at room temperature. The crude material was purified via column chromatography on a silica column (20:80 v/v EtOAc:CH_2Cl_2) to afford the title compound as an orange solid (0.0265 g, 0.060 mmol, 60.4% yield). ^{1}H NMR (500 MHz, DMSO-d_6) δ 10.14 (s, 1H), 8.03 (s, 1H), 7.98 (d, J = 7.8 Hz, 1H), 7.76 (d, J = 6.9 Hz, 1H), 7.52 (d, J = 7.7 Hz, 1H), 6.81 (d, J = 10.9 Hz, 1H), 6.63 (d, J = 11.1 Hz, 1H), 6.55 (d, J = 7.0 Hz, 1H), 6.01 (s, 2H), 2.14 (s, 3H), 2.13 (s, 3H). ^{13}C NMR (125 MHz, DMSO-d_6) δ 193.51, 175.18 (d, J = 20.8 Hz), 169.80, 157.56 (t, d, J = 5.1 Hz), 155.16 (d, J = 265.5

DOI: 10.1021/acscentsci.8b00313
ACS Cent. Sci. 2018, 4, 1045−1055

Hz), 148.82 (d, J = 245.5 Hz), 149.12, 148.91 (d, J = 12.5 Hz), 147.81 (d, J = 9.8 Hz), 137.33, 137.23, 137.14, 131.55, 130.02, 127.44, 117.80 (d, J = 8.5 Hz), 113.98 (d, J = 7.7 Hz), 113.02 (d, J = 21.5 Hz), 109.73 (d, J = 21.8 Hz), 105.77 (d, J = 4.8 Hz), 104.62, 84.80, 20.58, 19.00. $[M + H]^+$ Calc. mass for $C_{24}H_{17}O_6F_2$ = 439.0993; Found mass = 439.1008.

ALDH Isoform Activity Assays. The activity of each isoform of ALDH was confirmed by monitoring the production of NADH at 340 nm when incubated with the most commonly used substrate for that enzyme (propionaldehyde for ALDH1A1, ALDH1A2, ALDH1A3, ALDH2, and ALDH4A1; benzaldehyde for ALDH3A1, and succinic semialdehyde for ALDH5A1). Each isoform was diluted with 50 mM triethanolamine (TEA, pH 7.4) to a final concentration of 1 μM and placed in a 1 mL quartz cuvette. Directly before measurement, NAD^+ was added to final concentration of 2.5 mM, and the preferred substrate was added to a final concentration of 1 mM. Absorbance spectra were taken from 300 to 500 nm every half minute for 15 min. Units of activity for each enzyme were calculated from the slope of absorbance increase at 340 nm over time, (1 unit = 1 μmol substrate turned over/ μmol enzyme/min).

AlDeSense Isoform Selectivity Assay. Activation of AlDeSense was assessed using 20 units of each ALDH isoform. Activity was determined by activity measurements using each isoform's preferred substrate (1 unit = 1 μmol substrate turned over/μmol enzyme/min). Further details are in the Supporting Information. All enzymatic reactions were performed in 50 mM triethanolamine buffer (pH 7.4, Thermo Fisher) with 2.5 mM NAD^+ (Alfa Aesar) and 5% v/v DMSO (Thermo Fisher) in a 1 mL quartz cuvette at room temperature.

AlDeSense activation was determined using fluorescence. Immediately before measurement, AlDeSense (1 μM) was added to a quartz cuvette. After vigorous mixing, the reaction was monitored at room temperature for 15 min. Fluorescence spectra were acquired according to following parameters: λ_{ex} = 498 nm, and emission range = 505−580 nm. All scans were normalized to the signal from AlDeSense in 50 mM TEA and 2.5 mM NAD^+ (without enzyme). End point measurements at 15 min were performed in triplicate and reported as the averages ± standard deviation.

Inhibition of ALDH1A1. ALDH1A1 (100 nM) in 50 mM TEA (pH 7.4) was incubated with 2.5 mM NAD^+. Immediately before measurement, 4-diethylaminobenzaldehyde (DEAB) in 95% ethanol was added for a final concentration of 100 nM. The reaction was initiated with the addition of AlDeSense (1 μM). The solution was mixed with vigorous pipetting and fluorescence spectra were acquired. Fluorescence spectra were acquired according to following parameters: λ_{ex} = 498 nm, and emission range = 505−580 nm. Scans were taken periodically for up to 30 min. The reaction proceeded at room temperature throughout the experiment. All scans were normalized to the peak of AlDeSense in 50 mM TEA and 2.5 mM NAD^+ without the addition of enzyme.

siRNA Knockdown of ALDH1A1. K562 cells were grown to ∼70% confluency in a poly-L-lysine (Trevigen) coated Nunc Lab-Tek 8-well Chamber Slide system (Thermo Scientific) 1 day before treatment with siRNA. Both the negative control scrambled siRNA (Sigma-Aldrich, MISSION siRNA Universal Negative Control #1) as well as the ALDH1A1 siRNA (Sigma-Aldrich, SASI_Hs01_00244056) was applied at 50 μM concentrations following the Lipofectamine 3000 (Thermo Fisher) protocol for a 24-well plate. 0.75 μL of the Lipofectamine 3000 reagent was used per sample. After treatment, cells incubated with the siRNA in Opti-MEM (Gibco) at 37 °C, 5% CO_2 for 8 h. At this point, the Opti-MEM was removed and replaced with full growth media (IMDM supplemented with 10% FBS). Cells were incubated further at 37 °C, 5% CO_2 for 48 h before imaging on the Zeiss LSM 700 confocal. To stain the cells with each imaging reagent, 1 μL of 2 mM AlDeSense AM in DMSO was used per 1 mL of serum-free media (DMEM/F12 supplemented with 15 μM HEPES). Growth media was removed from the cells and replaced with the premixed dye solution. Cell staining continued for 30 min at room temperature (25 °C), after which the cells were immediately imaged. The optical configuration was optimized for the scrambled siRNA samples and the same optical settings were used for all images.

Mammosphere Culture and Imaging. Mammosphere formation from MDA-MB-231 breast cancer cells was performed as described previously with some modifications. Cells were resuspended and diluted to a density of 2000 cells/mL in DMEM/F12 (Sigma-Aldrich) supplemented with 2% B27 supplement (Thermo Fisher), 40 ng/mL rhFGF-2 (Miltenyi Biotec), and 20 ng/mL rhEGF (Gibco). They were plated in ultralow attachment six-well plates (Corning) and incubated at 37 °C and 5% CO_2 for 5 days or until most mammospheres were between 60 and 100 nm. At this point, the mammospheres were transferred to a four-well chamber slide coated with Poly-L-lysine as described previously. The mammospheres were then either immediately imaged with AlDeSense or Ctrl-AlDeSense, or the media was exchanged with full DMEM media supplement with 10% FBS and nonessential amino acids to allow differentiation over 36 h.

At various time points, the mammospheres were stained with 2 μM AlDeSense or Ctrl-AlDeSense as described above. Staining continued for 1 h at room temperature before imaging with a wide field fluorescence microscope (Zeiss Axiovert 200M). A GFP filter set was used to excite the fluorophores. Exposure times were set equally for all images taken within a data set and configured to give low signal in Ctrl-AlDeSense stained tumorspheres. Only mammospheres greater than 50 μm in diameter were considered in the analysis.

B16F0Melanoma Confocal Imaging. B16F0 murine melanoma cells were cultured for 5 days on polyacrylamide hydrogels with or without spiral patterns as described previously.[18] The coverslips on which the hydrogels and cells were mounted were transferred to a glass-bottomed dish for confocal imaging, leaving the cells intact. Solutions of either 2 μM AlDeSense AM or 2 μM Ctrl-AlDeSense AM in PBS were added to the two types of cells. The cells were incubated at room temperature for 1 h and then immediately imaged. Confocal imaging was performed on a Zeiss LSM700 Confocal Microscope, utilizing the 488 nm laser line to excite AlDeSense AM and the 20X/0.8 objective. Three different coverslips of cells were imaged for each set of conditions and at least six images were taken for each coverslip. Using ImageJ, ROIs were drawn around areas covered with cells and mean fluorescence values were measured for each image.

Ex Vivo Lung Metastases Imaging. Six- to eight-week-old female C57BL/6J mice were purchased from Jackson Laboratory. Experimental metastases were established by injecting 2 × 105 melanoma cells via lateral tail vein injection. Mice were euthanized at either 7 or 11 days post injection. Immediately after euthanization, their lungs were excised and

DOI: 10.1021/acscentsci.8b00313
ACS Cent. Sci. 2018, 4, 1045−1055

perfused with about 1 mL of either 15 μM AlDeSense AM or 15 μM Ctrl-AlDeSense AM in PBS. Outer portions of the lungs were rinsed in 15 mL of PBS to remove blood or excess dyes. After 2 h incubation at room temperature (25 °C), the lungs were imaged on the IVIS spectrum imaging system (PerkinElmer). Data were processed using Living Image software (Version 4.1).

In Vivo Melanoma Tumor Fluorescence Imaging. All in vivo imaging experiments were performed with the approval of the Institutional Animal Care and Use Committee of the University of Illinois at Urbana−Champaign. Six- to eight-week-old female BALB/c mice were purchased from the Jackson Laboratory for the tumor imaging experiment. Primary localized tumors were established by subcutaneously injecting B16F0 cells (5×10^5 cells in 100 μL of Hanks' balanced salt solution per injection). For each animal, cells that were grown on patterned gels were injected on the right lateral flank and cells grown on nonpatterned gels were injected on the left lateral flank. At 1 and 2 weeks, mice were intravenously injected with either 15 μM AlDeSense or Ctrl-AlDeSense. After 24 h, the mice were imaged using an IVIS spectrum imaging system for epifluorescence in conjunction with a CT scan. Data was processed using Living Image software (Version 4.1).

■ ASSOCIATED CONTENT

Supporting Information

The Supporting Information is available free of charge on the ACS Publications website at DOI: 10.1021/acscentsci.8b00313.

Experimental details, including synthetic procedures for Ctrl-AlDeSense and Ctrl-AlDeSense AM (PDF)

■ AUTHOR INFORMATION

Corresponding Author

*E-mail: jeffchan@illinois.edu.

ORCID

Lawrence W. Dobrucki: 0000-0002-6807-217X

Jefferson Chan: 0000-0003-4139-4379

Author Contributions

$^{\nabla}$C.A., J.H., and T.E.B. contributed equally.

Notes

Safety statement: No unexpected or unusually high safety hazards were encountered.

The authors declare no competing financial interest.

■ ACKNOWLEDGMENTS

This work was supported by the Chemistry-Biology Interface Training Grant (T32 GM070421 to C.A. and N.W.P.), the National Science Foundation Graduate Research Fellowship Program (DGE − 1144245 to C.A.), the Robert C. and Carolyn J. Springborn Graduate Fellowship (to C.A. and N.W.P.), the National Institute of Biomedical Imaging and Bioengineering Training Grant (T32EB019944 to J.H.), the Beckman Postdoctoral Fellowship (to J.H.), the Alfred P. Sloan Foundation MPHD Fellowship (to N.W.P.), and the Alfred P. Sloan fellowship (FG-2017-8964 to J.C.). Major funding for the 500 MHz Bruker CryoProbeTM was provided by the Roy J. Carver Charitable Trust (Muscatine, Iowa; Grant No. 15-4521) to the School of Chemical Sciences NMR Lab. The Q-T of Ultima mass spectrometer was purchased in part with a grant from the National Science Foundation, Division of Biological Infrastructure (DBI-0100085). We thank the Core Facilities at the Carl R. Woese Institute for Genomic Biology for access to the Zeiss LSM 700 Confocal Microscope and corresponding software. We acknowledge Dr. Iwona Dobrucka and the Molecular Imaging Laboratory at the Beckman Institute for use of the IVIS imaging system. We thank Dr. Barbara Pilas and the Flow Cytometry Facility for help with data analysis. We thank Dr. Sandra McMasters and the Cell Media Facility for assistance preparing cell culture media and advising on growth conditions. We thank Professor Daria Mochly-Rosen and Dr. Che-Hong Chen for ALDH plasmids. We thank Professor Tom Hurley for consultation on the crystal structure.

■ REFERENCES

(1) Bonnet, D.; Dick, J. E. Human Acute Myeloid Leukemia Is Organized as a Hierarchy That Originates from a Primitive Hematopoietic Cell. *Nat. Med.* **1997**, *3*, 730−737.

(2) Zubair, H.; Azim, S.; Srivastava, S. K.; Bhardwaj, A.; Marimuthu, S.; Patton, M. C.; Singh, S.; Singh, A. P. Cancer Stem Cells: Concept, Significance, and Management. In *Stem Cells in Toxicology and Medicine*; Sahu, S. C., Ed.; John Wiley & Sons, Ltd: Chichester, UK, 2016; pp 375−413.

(3) Skvortsova, I.; Debbage, P.; Kumar, V.; Skvortsov, S. Radiation Resistance: Cancer Stem Cells (CSCs) and Their Enigmatic Pro-survival Signaling. *Semin. Cancer Biol.* **2015**, *35*, 39−44.

(4) Begicevic, R.-R.; Falasca, M. ABC Transporters in Cancer Stem Cells: Beyond Chemoresistance. *Int. J. Mol. Sci.* **2017**, *18*, 2362, .

(5) Pallini, R.; Ricci-Vitiani, L.; Montano, N.; Mollinari, C.; Biffoni, M.; Cenci, T.; Pierconti, F.; Martini, M.; De Maria, R.; Larocca, L. M. Expression of the Stem Cell Marker CD133 in Recurrent Glioblastoma and Its Value for Prognosis. *Cancer* **2011**, *117*, 162−174.

(6) Heryanto, Y. D.; Achmad, A.; Taketomi-Takahashi, A.; Tsushima, Y. In Vivo Molecular Imaging of Cancer Stem Cells. *Am. J. Nucl. Med. Mol. Imaging* **2015**, *5*, 14−26.

(7) Kise, K.; Kinugasa-Katayama, Y.; Takakura, N. Tumor Microenvironment for Cancer Stem Cells. *Adv. Drug Delivery Rev.* **2016**, *99*, 197−205.

(8) Plaks, V.; Kong, N.; Werb, Z. The Cancer Stem Cell Niche: How Essential Is the Niche in Regulating Stemness of Tumor Cells? *Cell Stem Cell* **2015**, *16*, 225−238.

(9) Lau, E. Y.-T.; Ho, N. P.-Y.; Lee, T. K.-W. Cancer Stem Cells and Their Microenvironment: Biology and Therapeutic Implications. *Stem Cells Int.* **2017**, *2017*, 3714190.

(10) Gaedicke, S.; Braun, F.; Prasad, S.; Machein, M.; Firat, E.; Hettich, M.; Gudihal, R.; Zhu, X.; Klingner, K.; Schüler, J.; Herold-Mende, C. C.; Grosu, A.-L.; Behe, M.; Weber, W.; Mäcke, H.; Niedermann, G. Noninvasive Positron Emission Tomography and Fluorescence Imaging of CD133+ Tumor Stem Cells. *Proc. Natl. Acad. Sci. U. S. A.* **2014**, *111*, E692−701.

(11) Clevers, H. The Cancer Stem Cell: Premises, Promises and Challenges. *Nat. Med.* **2011**, *17*, 313−319.

(12) Xenaki, K. T.; Oliveira, S.; van Bergen En Henegouwen, P. M. P. Antibody or Antibody Fragments: Implications for Molecular Imaging and Targeted Therapy of Solid Tumors. *Front. Immunol.* **2017**, *8*, 1287.

(13) Thurber, G. M.; Schmidt, M. M.; Wittrup, K. D. Factors Determining Antibody Distribution in Tumors. *Trends Pharmacol. Sci.* **2008**, *29*, 57−61.

(14) Liu, H.; Patel, M. R.; Prescher, J. A.; Patsialou, A.; Qian, D.; Lin, J.; Wen, S.; Chang, Y.-F.; Bachmann, M. H.; Shimono, Y.; Dalerba, P.; Adorno, M.; Lobo, N.; Bueno, J.; Dirbas, F. M.; Goswami, S.; Somlo, G.; Condeelis, J.; Contag, C. H.; Gambhir, S. S.; Clarke, M. F. Cancer Stem Cells from Human Breast Tumors Are

DOI: 10.1021/acscentsci.8b00313
ACS Cent. Sci. 2018, 4, 1045−1055

Involved in Spontaneous Metastases in Orthotopic Mouse Models. *Proc. Natl. Acad. Sci. U. S. A.* **2010**, *107*, 18115−18120.
(15) Fink, J.; Andersson-Rolf, A.; Koo, B.-K. Adult Stem Cell Lineage Tracing and Deep Tissue Imaging. *BMB Rep* **2015**, *48*, 655−667.
(16) Rycaj, K.; Tang, D. G. Cell-of-Origin of Cancer Versus Cancer Stem Cells: Assays and Interpretations. *Cancer Res.* **2015**, *75*, 4003−4011.
(17) Zhou, L.; Jiang, Y.; Yan, T.; Di, G.; Shen, Z.; Shao, Z.; Lu, J. The Prognostic Role of Cancer Stem Cells in Breast Cancer: a Meta-analysis of Published Literatures. *Breast Cancer Res. Treat.* **2010**, *122*, 795−801.
(18) Pors, K.; Moreb, J. S. Aldehyde Dehydrogenases in Cancer: An Opportunity for Biomarker and Drug Development? *Drug Discovery Today* **2014**, *19*, 1953−1963.
(19) Li, T.; Su, Y.; Mei, Y.; Leng, Q.; Leng, B.; Liu, Z.; Stass, S. A.; Jiang, F. ALDH1A1 Is a Marker for Malignant Prostate Stem Cells and Predictor of Prostate Cancer Patients' Outcome. *Lab. Invest.* **2010**, *90*, 234−244.
(20) Li, X.; Wan, L.; Geng, J.; Wu, C.-L.; Bai, X. Aldehyde Dehydrogenase 1A1 Possesses Stem-like Properties and Predicts Lung Cancer Patient Outcome. *J. Thorac. Oncol.* **2012**, *7*, 1235−1245.
(21) Khoury, T.; Ademuyiwa, F. O.; Chandraseekhar, R.; Jabbour, M.; Deleo, A.; Ferrone, S.; Wang, Y.; Wang, X. Aldehyde Dehydrogenase 1A1 Expression in Breast Cancer Is Associated with Stage, Triple Negativity, and Outcome to Neoadjuvant Chemotherapy. *Mod. Pathol.* **2012**, *25*, 388−397.
(22) Januchowski, R.; Wojtowicz, K.; Sterzylska, K.; Sosilska, P.; Andrzejewska, M.; Zawierucha, P.; Nowicki, M.; Zabel, M. Inhibition of ALDH1A1 Activity Decreases Expression of Drug Transporters and Reduces Chemotherapy Resistance in Ovarian Cancer Cell Lines. *Int. J. Biochem. Cell Biol.* **2016**, *78*, 248−259.
(23) Vasiliou, V.; Pappa, A.; Petersen, D. R. Role of Aldehyde Dehydrogenases in Endogenous and Xenobiotic Metabolism. *Chem.-Biol. Interact.* **2000**, *129*, 1−19.
(24) Vasiliou, V.; Nebert, D. W. Analysis and Update of the Human Aldehyde Dehydrogenase (ALDH) Gene Family. *Human Genomics* **2005**, *2*, 138143
(25) Storms, R. W.; Trujillo, A. P.; Springer, J. B.; Shah, L.; Colvin, O. M.; Ludeman, S. M.; Smith, C. Isolation of Primitive Human Hematopoietic Progenitors on the Basis of Aldehyde Dehydrogenase Activity. *Proc. Natl. Acad. Sci. U. S. A.* **1999**, *96*, 9118−9123.
(26) Minn, I.; Wang, H.; Mease, R. C.; Byun, Y.; Yang, X.; Wang, J.; Leach, S. D.; Pomper, M. G. A Red-shifted Fluorescent Substrate for Aldehyde Dehydrogenase. *Nat. Commun.* **2014**, *5*, 3662.
(27) Yagishita, A.; Ueno, T.; Esumi, H.; Saya, H.; Kaneko, K.; Tsuchihara, K.; Urano, Y. Development of Highly Selective Fluorescent Probe Enabling Flow-Cytometric Isolation of ALDH3A1-Positive Viable Cells. *Bioconjugate Chem.* **2017**, *28*, 302−306.
(28) Morgan, C. A.; Parajuli, B.; Buchman, C. D.; Dria, K.; Hurley, T. D. N,N-Diethylaminobenzaldehyde (DEAB) as a Substrate and Mechanism-based Inhibitor for Human ALDH Isoenzymes. *Chem.-Biol. Interact.* **2015**, *234*, 18−28.
(29) Luo, M.; Gates, K. S.; Henzl, M. T.; Tanner, J. J. Diethylaminobenzaldehyde Is a Covalent, Irreversible Inactivator of ALDH7A1. *ACS Chem. Biol.* **2015**, *10*, 693−697.
(30) Moreb, J. S.; Ucar, D.; Han, S.; Amory, J. K.; Goldstein, A. S.; Ostmark, B.; Chang, L.-J. The Enzymatic Activity of Human Aldehyde Dehydrogenases 1A2 and 2 (ALDH1A2 and ALDH2) Is Detected by Aldefluor, Inhibited by Diethylaminobenzaldehyde and Has Significant Effects on Cell Proliferation and Drug Resistance. *Chem.-Biol. Interact.* **2012**, *195*, 52−60.
(31) Marcato, P.; Dean, C. A.; Giacomantonio, C. A.; Lee, P. W. K. Aldehyde Dehydrogenase: Its Role as a Cancer Stem Cell Marker Comes down to the Specific Isoform. *Cell Cycle* **2011**, *10*, 1378−1384.
(32) Mottram, L. F.; Boonyarattanakalin, S.; Kovel, R. E.; Peterson, B. R. The Pennsylvania Green Fluorophore: a Hybrid of Oregon Green and Tokyo Green for the Construction of Hydrophobic and pH-insensitive Molecular Probes. *Org. Lett.* **2006**, *8*, 581−584.
(33) Ueno, T.; Urano, Y.; Setsukinai, K.-I.; Takakusa, H.; Kojima, H.; Kikuchi, K.; Ohkubo, K.; Fukuzumi, S.; Nagano, T. Rational Principles for Modulating Fluorescence Properties of Fluorescein. *J. Am. Chem. Soc.* **2004**, *126*, 14079−14085.
(34) Tanaka, F.; Mase, N.; Barbas, C. F. Design and Use of Fluorogenic Aldehydes for Monitoring the Progress of Aldehyde Transformations. *J. Am. Chem. Soc.* **2004**, *126*, 3692−3693.
(35) Izumi, S.; Urano, Y.; Hanaoka, K.; Terai, T.; Nagano, T. A Simple and Effective Strategy to Increase the Sensitivity of Fluorescence Probes in Living Cells. *J. Am. Chem. Soc.* **2009**, *131*, 10189−10200.
(36) Morgan, C. A.; Hurley, T. D. Development of a High-throughput in Vitro Assay to Identify Selective Inhibitors for Human ALDH1A1. *Chem.-Biol. Interact.* **2015**, *234*, 29−37.
(37) Liu, Z. J.; Hempel, J.; Sun, J.; Rose, J.; Hsiao, D.; Chang, W. R.; Chung, Y. J.; Kuo, I.; Lindahl, R.; Wang, B. C. Crystal Structure of a Class 3 Aldehyde Dehydrogenase at 2.6 Å Resolution. *Enzymol. Mol. Biol. Carbonyl Metab.* **1996**, *414*, 1−7.
(38) Steinmetz, C. G.; Xie, P.; Weiner, H.; Hurley, T. D. Structure of Mitochondrial Aldehyde Dehydrogenase: The Genetic Component of Ethanol Aversion. *Structure* **1997**, *5*, 701−711.
(39) Moretti, A.; Li, J.; Donini, S.; Sobol, R. W.; Rizzi, M.; Garavaglia, S. Crystal Structure of Human Aldehyde Dehydrogenase 1A3 Complexed with NAD+ and Retinoic Acid. *Sci. Rep.* **2016**, *6*, 35710.
(40) Wang, M.-F.; Han, C.-L.; Yin, S.-J. Substrate Specificity of Human and Yeast Aldehyde Dehydrogenases. *Chem.-Biol. Interact.* **2009**, *178*, 36−39.
(41) Wang, W.; Rusin, O.; Xu, X.; Kim, K. K.; Escobedo, J. O.; Fakayode, S. O.; Fletcher, K. A.; Lowry, M.; Schowalter, C. M.; Lawrence, C. M.; Fronczek, F. R.; Warner, I. M.; Strongin, R. M. Detection of Homocysteine and Cysteine. *J. Am. Chem. Soc.* **2005**, *127*, 15949−15958.
(42) Rusin, O.; St. Luce, N. N.; Agbaria, R. A.; Escobedo, J. O.; Jiang, S.; Warner, I. M.; Dawan, F. B.; Lian, K.; Strongin, R. M. Visual Detection of Cysteine and Homocysteine. *J. Am. Chem. Soc.* **2004**, *126*, 438−439.
(43) Feuster, E. K.; Glass, T. E. Detection of Amines and Unprotected Amino Acids in Aqueous Conditions by Formation of Highly Fluorescent Iminium Ions. *J. Am. Chem. Soc.* **2003**, *125*, 16174−16175.
(44) Bliss, S. A.; Paul, S.; Pobiarzyn, P. W.; Ayer, S.; Sinha, G.; Pant, S.; Hilton, H.; Sharma, N.; Cunha, M. F.; Engelberth, D. J.; Greco, S. J.; Bryan, M.; Kucia, M. J.; Kakar, S. S.; Ratajczak, M. Z.; Rameshwar, P. Evaluation of a Developmental Hierarchy for Breast Cancer Cells to Assess Risk-based Patient Selection for Targeted Treatment. *Sci. Rep.* **2018**, *8*, 367.
(45) Cui, X. Y.; Skretting, G.; Jing, Y.; Sun, H.; Sandset, P. M.; Sun, L. Hypoxia Influences Stem Cell-like Properties in Multidrug Resistant K562 Leukemic Cells. *Blood Cells, Mol., Dis.* **2013**, *51*, 177−184.
(46) Carnero, A.; Lleonart, M. The Hypoxic Microenvironment: A Determinant of Cancer Stem Cell Evolution. *BioEssays* **2016**, *38*, S65−S105.
(47) Thul, P. J.; Åkesson, L.; Wiking, M.; Mahdessian, D.; Geladaki, A.; Ait Blal, H.; Alm, T.; Asplund, A.; Björk, L.; Breckels, L. M.; Bäckström, A.; Danielsson, F.; Fagerberg, L.; Fall, J.; Gatto, L.; Gnann, C.; Hober, S.; Hjelmare, M.; Johansson, F.; Lee, S.; Lindskog, C.; Mulder, J.; Mulvey, C. M.; Nilsson, P.; Oksvold, P.; Rockberg, J.; Schutten, R.; Schwenk, J. M.; Sivertsson, Å.; Sjöstedt, E.; Skogs, M.; Stadler, C.; Sullivan, D. P.; Tegel, H.; Winsnes, C.; Zhang, C.; Zwahlen, M.; Mardinoglu, A.; Pontén, F.; von Feilitzen, K.; Lilley, K. S.; Uhlén, M.; Lundberg, E. A Subcellular Map of the Human Proteome. *Science* **2017**, *356*, eaal3321.
(48) Shaw, F. L.; Harrison, H.; Spence, K.; Ablett, M. P.; Simões, B. M.; Farnie, G.; Clarke, R. B. A Detailed Mammosphere Assay

DOI: 10.1021/acscentsci.8b00313
ACS Cent. Sci. 2018, 4, 1045−1055

Protocol for the Quantification of Breast Stem Cell Activity. *J. Mammary Gland Biol. Neoplasia* **2012**, *17*, 111−117.
(49) Lee, C.-H.; Yu, C.-C.; Wang, B.-Y.; Chang, W.-W. Tumorsphere as an Effective in Vitro Platform for Screening Anti-cancer Stem Cell Drugs. *Oncotarget* **2016**, *7*, 1215−1226.
(50) Lee, J.; Abdeen, A. A.; Wycislo, K. L.; Fan, T. M.; Kilian, K. A. Interfacial Geometry Dictates Cancer Cell Tumorigenicity. *Nat. Mater.* **2016**, *15*, 856−862.
(51) Guo, R.; Fierro-Fine, A.; Goddard, L.; Russell, M.; Chen, J.; Liu, C. Z.; Fung, K.-M.; Hassell, L. A. Increased Expression of Melanoma Stem Cell Marker CD271 in Metastatic Melanoma to the Brain. *Int. J. Clin. Exp. Pathol.* **2014**, *7*, 8947−8951.
(52) Redmer, T.; Walz, I.; Klinger, B.; Khouja, S.; Welte, Y.; Schäfer, R.; Regenbrecht, C. The Role of the Cancer Stem Cell Marker CD271 in DNA Damage Response and Drug Resistance of Melanoma Cells. *Oncogenesis* **2017**, *6*, No. e291.
(53) Woydziak, Z. R.; Fu, L.; Peterson, B. R. Efficient and Scalable Synthesis of 4-Carboxy-Pennsylvania Green Methyl Ester: A Hydrophobic Building Block for Fluorescent Molecular Probes. *Synthesis* **2014**, *46*, 158−164.

DOI: 10.1021/acscentsci.8b00313
ACS Cent. Sci. 2018, 4, 1045−1055